Available online at www.sciencedirect.com
ScienceDirect
Proceedings of the Combustion Institute 000 (2022) 1–10
Proceedings of the Combustion Institute
www.elsevier.com/locate/proci

How does a resilient, flexible ammonia process look? Robust design optimization of a Haber-Bosch process with optimal dynamic control powered by wind

Kevin Verleysen [a,b,c,*], Alessandro Parente [b,c], Francesco Contino [d]

[a] Thermo and Fluid Dynamics (FLOW), Vrije Universiteit Brussel (VUB), Brussels, Belgium
[b] Aero-Thermo-Mechanical Department (ATM), Université Libre de Bruxelles (ULB), Brussels, Belgium
[c] Brussels Institute for Thermal-Fluid Systems and clean Energy (BRITE), Vrije Universiteit Brussel (VUB) and Université Libre de Bruxelles (ULB), Belgium
[d] Institute of Mechanics, Materials and Civil Engineering (iMMC), Université catholique de Louvain (UCLouvain), Louvain-la-Neuve, Belgium

Received 5 January 2022; accepted 23 June 2022

Abstract

Ammonia can be an essential energy vector for storing excess renewable energy during the year and release this energy when demand is high. This storage during the year provides an essential part in the energy sector for moments when there is not enough wind and sun to cover the demand. Although the Haber-Bosch is a very mature process to synthesize hydrogen and nitrogen to ammonia, it is not flexible enough to match the erratic nature of renewables. This mismatch creates the need for large intermediate hydrogen buffer tanks. To reduce the capacity of the hydrogen storage tank, we need to optimize the dynamic power-to-ammonia process in a minute time scale while considering the uncertainties linked to renewables. Therefore, we coupled a stochastic wind power process to a dynamic Power-to-Ammonia process and performed a design optimization under uncertainties, i.e. a robust design optimization, for a three-hour wind scenario while considering optimal dynamic control. The robust design optimization showed significant trade-offs between the most productive, the most flexible, the most resilient, and robust power-to-ammonia plant designs. For the flexible and productive designs, the bypass fraction and buffer feed have essential roles in achieving these designs. In the future, we will use a stochastic process to consider the uncertainty of renewable power over more extended periods (days, weeks and months) coupled with the robust design optimization of the dynamic power-to-ammonia process and investigate its effect on the intermediate hydrogen buffer size and the plant's cost.

Keywords: Ammonia synthesis; Dynamic Haber-Bosch; Robust design optimization; Stochastic process

1. Introduction

To create a sustainable future and reduce our global carbon emissions, we need to integrate renewables further into our society. Solar, wind, hydropower and bioenergy are the leading

* Corresponding author at: Thermo and Fluid Dynamics (FLOW), Vrije Universiteit Brussel (VUB), Brussels, Belgium.
E-mail address: kevin.verleysen@vub.be (K. Verleysen).

https://doi.org/10.1016/j.proci.2022.06.027
1540-7489

Please cite this article as: K. Verleysen, A. Parente and F. Contino, How does a resilient, flexible ammonia process look? Robust design optimization of a Haber-Bosch process with optimal dynamic control powered by wind, Proceedings of the Combustion Institute, https://doi.org/10.1016/j.proci.2022.06.027

renewable electricity production methods [1]. Wind and solar can be implemented everywhere (residential, rural or islanded areas) and are popularized by the cost reduction of the turbine and photovoltaic panels combined with government incentives [1]. However, a significant problem with wind and solar power is the non-dispatchable nature and erratic behavior of these energy sources. In addition, these energy sources have different variability over various time scales (from seconds to months), where seasonality could play a critical role in securing the energy supply over the year [2]. Therefore, we can chemically store the excess renewable energy in a fuel over the year and use this fuel later in a power plant when needed.

A trending primary chemical that can be produced easily by renewables and used as a fuel is hydrogen (H_2). Hydrogen can be produced via alkaline, Polymer Exchange Membrane (PEM), or solid oxide electrolyzers and relatively efficiently converted back to electricity via fuel cells or combined cycles gas turbines [3]. However, storage over a long period (months) and transport over a long distance (>1000 km) is a bottleneck in this energy vector's cheap and long-term storage. The capital cost of hydrogen gas storage varies between 400 USD/kgH_2 and 1400 USD/kgH_2 (6 USD/kWh and 45 USD/kWh) depending on the storage pressure and size [4,5]. These storage costs can be circumvented by combining the renewable hydrogen gas with nitrogen (N_2) gas in the presence of a catalyst at high temperature and pressure in the Haber-Bosch Synthesis (HBS) process to produce ammonia (NH_3). The storage of NH_3 is only 0.875 USD/kgNH_3 (0.14 USD/kWh) [4] which significantly reduces the capital cost for large-scale, long-term H_2 storage while relying on a mature technology. Ammonia is currently used as the primary source of fertilizers, but in the future shows potential as a fuel in compression ignition or spark ignition engines [6].

This concept to store renewable energy in NH_3 is the Power-to-Ammonia (PtA) process. A PtA plant is typically divided into three components. The most significant part of the power (≈92% [7]) is used to power an electrolyzer. Around 2% of the power is used to separate N_2 gas from the air with an Air Separation Unit (ASU). The residual power is used to synthesize the H_2 and N_2 to NH_3 [7,8]. While the PEM electrolyzer can be quickly shut down, start-up and ramp-up/-down, the HBS process has its operational limits in practice. The start-up procedure of this HBS process requires up to several days to go to the nominal operation. In addition, ramping the inlet flow (the hydrogen and nitrogen mixture) is limited to 20%/h of the nominal flow with current technologies [5,9]. Above this ramp limit constraint, the thermal changes could extensively damage the catalyst in the Haber-Bosch [10]. To avoid the shutdown of a PtA plant, there is a need to install large hydrogen and nitrogen buffer tanks and a backup system. With these buffer tanks, the continuation of the ammonia is guaranteed and the shutdown is avoided, but with an increased capital cost [5].

Typical PtA studies investigate the Levelized Cost of Ammonia (LCOA) to find the most economical system at various locations and case studies like the work of Armijo and Philibert [5], Allman and Daoutidis [11] and Nayak-Luke et al. [12]. These studies limited the ramp-up rate but only considered steady-state linearized models. Cheema and Krewer [13] investigated the influence of key operational parameters to extend the load range of the HBS process. However, these studies did not include the actual non-linear dynamic behavior of the Haber-Bosch process, like in the work of Wang et al. [14]. This work showed the importance of considering a dynamic ammonia synthesis model when powered by renewables as the optimal steady-state conditions are not favorable for the flexible operation of the plant over time. A significant difficulty with changing the load of the HBS process is the tendency to initiate oscillatory behavior in the autothermal reactor [15]. For this reason, an adapted control structure is needed to avoid these instabilities while keeping the plant operation stable [16] or economic [17]. Despite the highly nonlinear behavior of the NH_3 synthesis process, the effect of uncertainties is rarely discussed [18]. The traditional design and operation of PtA systems assume deterministic performance over time, while in reality, uncertainties can significantly affect the average yearly NH_3 production [7] and during load ramping [8].

To account for the intermittent effect of renewables, we can use a Stochastic Differential Equation (SDE) during the design of the dynamic PtA system. These SDEs can capture the variability of renewables by creating different scenarios according to real measured data [19]. Combining these stochastic processes with optimization is attractive for designing controllers in power systems under renewable energy source uncertainties [20,21].

This paper aims to design a dynamic PtA system under wind power uncertainties using an SDE and optimize its production, flexibility and resilience against these temporal variations. We investigate this design optimization under uncertainties, i.e., robust design optimization, where we excluded the ramp limit of 20%/h to observe the advantage of a limitless PtA process.

2. Modeling the wind to ammonia process

This section presents each process for assessing the effect of uncertain wind power on the dynamic PtA process. The first subsection describes the SDE for the wind power scenarios and the application of the Karhunen-Loève Expansion with Polynomial Chaos Expansion. Then, the main components in the Power-to-Ammonia model are presented. Next, the power management strategy is defined to control the power towards the three components of the PtA process.

2.1. Stochastic wind power process

Stochastic processes provide a tool to determine the effect of variability in renewable energy sources on power systems and design the necessary controllers to reduce these effects [20]. The Itȳ process can describe these stochastic processes with a general equation $dX_t = a(t, X_t)dt + b(t, X_t)dW_t$ which has the potential to describe any Gaussian and non-Gaussian process X at time t with a differential equation characterized by the Wiener process W_t (a standard Brownian motion), a drift term a and a diffusion term b. The drift and diffusion terms can take different forms and uses, like describing the trends and volatility in financial models [22,23], in physical systems [24] or, for our case, renewable energy sources, like wind and solar power [25,26].

In recent years, a particular stochastic differential equation has been used to model the variability of wind speed and wind power based on real measurement data [19,21]. This SDE is called the Ornstein-Uhlenbeck (OU) process (Eq. (1)).

$$dY_t = -\eta Y_t dt + \nu dW_t \tag{1}$$

This SDE equation represents a Gaussian stochastic process Y_t with a normal distribution, a zero mean and a variance of $\nu^2/2\eta$. Verdejo et al. [19] and Loukatou et al. [27] used this OU stochastic process to respectively generate wind power data sets for short-term (hours) or wind speed for long-term (one month) scenarios based on real wind data. We adopted the η (-8.707802) and ν (0.2309347) parameters described in Verdejo et al. [19] to model the stochastic power output of a wind farm in Chile. These parameters are obtained from real wind power data where the parameter estimation process is calculated with the following equations [19]:

$$\widetilde{\eta} = \frac{1}{\Delta t} \log \frac{\sum_{i=1}^{n} Y_{(i-1)\Delta t} Y_{i\Delta t}}{\Sigma_{i=1}^{n} Y_{(i-1)\Delta t}^2} \tag{2}$$

and

$$\widetilde{\nu} = \sqrt{\frac{1}{n\Delta t} \sum_{i=1}^{n} (Y_{i\Delta t} - Y_{(i-1)\Delta t})^2} \tag{3}$$

where Δt is the time interval between two observations and $Y_{i\Delta t}$ represents the observed value at time $i\Delta t$. Before these parameter estimation equations can be applied, the observed wind power data (X_t) needs to be transformed to fit the characteristics of the OU process (zero mean and normal distribution). Verdejo et al. suggest linking the observed wind power (X_t) to the OU process (Y_t) with the following normal-logarithmic function:

$$X_t = e^{Y_t + h}, \tag{4}$$

where h represents the mean of $\ln Y_t$, which is for this case 9.633223 [19]. This transformation allows the wind data to have a zero mean and a small variance [19]. For our application, we only look at the OU process to simulate a random path (with Y_t) where afterward this path is transformed to power (X_t) with Eq. (4). For the adopted OU model and parameters (η, ν and h), we observed a mean electric power output of 15.7 MW and a standard deviation of 0.84 MW with a Monte-Carlo(MC)-based simulation. To the high average wind power over these three hours, we did not consider a backup system, e.g. grid or battery, to compensate for the absence of wind power.

Stochastic processes can be solved with different numerical integration schemes, where the Euler-Maruyama and the Milstein schemes are the most used ones [28]. For the OU process, a Milstein integration method shows a stronger convergence towards the expected mean and standard deviation [29,30]. However, these integration schemes involve sampling a standard normal distribution at each time step. An MC sampling technique is traditionally used to converge toward the true solution of a stochastic process. This technique needs to be avoided as it would require >10^6 paths for each design in the context of robust design optimization of dynamic models. Alternatively, Polynomial Chaos Expansion (PCE) is a more attractive method to perform this sampling over each timestep since it significantly reduces the number of samples compared to the MC approach. This PCE method represents the stochastic process Y_t with a surrogate model M which is a truncated series of multivariate orthonormal polynomials $\mathbf{\Phi}_i(\xi_t)$ obtained by the tensor product of univariate polynomials and the associated deterministic coefficients y_i such that $Y_t \approx M(\xi_t) = \sum_{i=0}^{P} y_i(t)\mathbf{\Phi}_i(\xi_t)$. However, the paper of Di Persio et al. shows that the direct application of the PCE to the OU process requires one uncertainty for each timestep [31]. This method results in an exponential increase of samples as the number of PCE terms are linked to $P + 1 = (n + p)!/(n!p!)$, where n is the number of uncertainties (number of time steps) and p the polynomial order. To circumvent these large quantities of uncertainties, we can orthogonally decompose the OU process into a series of independent standard Gaussian random variables with the so-called Karhunen-Loève Expansion (KLE) [26]. This KLE is a proper orthogonal decomposition method typically for stochastic processes [32]. Analogous to the KLE of the Wiener process, we can define the KLE of a stochastic process by the infinite sum of a standard normal distribution ξ, the eigenfunction e and the eigenvalue λ (Eq. (5)).

$$Y_t = \sum_{j=1}^{\infty} \xi_j e_j(t) \sqrt{\lambda_j} \tag{5}$$

Corlay and Pagès [33] derived the eigenfunctions $e_j(t)$ and eigenvalues λ_j for each term of the Ornstein-Uhlenbeck process in the KLE form with:

$$e_j(t) = \frac{\sin(\omega_j t)}{\sqrt{\frac{t_{end}}{2} - \frac{\sin(2\omega_j)t_{end}}{4\omega_j}}} \quad j \geq 1, \tag{6}$$

and

$$\lambda_j = \frac{\nu^2}{\omega_j^2 + \eta^2} \quad j \geq 1, \tag{7}$$

while providing a technique to determine ω_j (Eq. (8)).

$$\eta \tan(\omega_j t_{end}) + \omega_j = 0. \tag{8}$$

For each ω_j, a unique solution needs to be found in each interval $[\pi j/t_{end} - \pi/(2t_{end}), \pi j/t_{end}]$ for $j = 1, 2, \ldots, \infty$, where t_{end} is the final time. To attain the computational effort low, the KLE needs to be truncated to order N, which is a trade-off between computational efficiency and accuracy (Eq. (9)).

$$Y_t = \sum_{j=1}^{N} \xi_j e_j(t) \sqrt{\lambda_j} \tag{9}$$

From the KLE of the OU process, we applied the PCE method to quantify the mean and standard deviation at each time step. We then compared the expected wind power and the wind power statistics via the KLE-PCE algorithm over a 3-hour scenario with a timestep of 1 min. We observed that the average relative error of the mean and standard deviation over the 3-hour scenario decreases when the number of uncertainties increases. For instance, 50 uncertainties provide an average error of 0.030% and 5.95% on the mean and standard deviation. With 100 uncertainties, the average errors decreased to 0.021% and 2.88%. We choose 100 uncertainties (N) for our case because of the trade-off between computational effort and accuracy.

2.2. Power-to-ammonia

The electrolyzer, the air separation unit and the intermediate buffer tank models are presented. Next, the dynamic Haber-Bosch process is described and the reactor configuration is provided. Finally, the power management strategy is given.

2.2.1. H_2 and N_2 production and buffer

We adopted a PEM electrolyzer and a Pressure Swing Adsorption (PSA) model to deal with the intermittent wind power. These PEM and PSA processes are typically chosen in the PtA concept for their modular sizing and the flexibility required to be connected to an erratic energy source [34]. We assumed linear steady-state models and disregarded the voltage-current relationship for PEM and adsorption and purge steps for the PSA to limit the computational cost of each timestep to 3 s. For the PEM electrolyzer, we adopted the model of Kaviani et al. [35] to transform the electric energy in hydrogen gas (Eq. (10)):

$$\dot{m}_{\mathrm{H_2}} = \frac{P_{\mathrm{PEM}}}{\eta_{\mathrm{PEM}}\ \mathrm{HHV_{H_2}}} \quad [\mathrm{kg/s}], \tag{10}$$

where P_{PEM} is the electrolyzer power in MW, η_{PEM} is the electrolyzer efficiency (0.79) and $\mathrm{HHV_{H_2}}$ is the Higher Heating Value of H_2 (142 MJ/kg). For the PSA process, the nitrogen gas production $\dot{m}_{\mathrm{N_2}}$ is proportionally linked to the power to the PSA P_{PSA} with Eq. (11) [16,36].

$$\dot{m}_{\mathrm{N_2}} = \frac{P_{\mathrm{PSA}}\eta_{\mathrm{PSA}}}{c_p T_{\mathrm{amb}}\left[\left(\frac{p_o}{p_i}\right)^{(R/c_p)} - 1\right]} \quad [\mathrm{kg/s}] \tag{11}$$

In this equation, η_{PSA} is the efficiency (0.72) of the PSA, c_p the heat capacity of air (29.03 kJ/kmolK), T_{amb} the ambient air temperature, $p_{o/i}$ is the output/input pressure (40 bar and 1 bar), R is the gas constant of air (8.314 kJ/kmol).

Both processes produce gasses that must be (partially) buffered before entering the Haber-Bosch loop. For this part of the process, we implemented a hydrogen bypass line to allow the design optimizer to size the fraction of H_2 directly fed to the Haber-Bosch while the residual part is stored in the H_2 buffer tank. In addition, the optimizer decides how much H_2 gas is extracted from the buffer tank to provide a minimal constant flow towards the HBS process. For the produced N_2 gas, we store all the gas directly in a buffer tank. When the H_2 feed to the HBS process is known, we extract one mol of N_2 for each three mol of H_2.

2.2.2. Ammonia production

A Haber-Bosch loop converts the hydrogen/nitrogen mixture into ammonia. This chemical process consists of four typical components: a compressor to pressurize the mixture to the operational pressure, an auto-thermal reactor to synthesize the gas mixture to NH_3, a separation system to extract the NH_3 from the loop and a recycle loop to reuse the unreacted H_2 and N_2 gas (Fig. 1). We created a Python library for these components based on the GEKKO framework [37]. GEKKO allows machine learning and optimization of mixed-integer and differential-algebraic equations. The framework contains a variety of nonlinear programming solvers and different modes to simulate the steady-state and dynamic behavior of models [37]. With this library, we simulated the dynamic behavior of our chosen Haber-Bosch process at a minute time scale. The complete Haber-Bosch loop contains a loop compressor (C_1), a preheater (H), a specific reactor configuration (Reactor), a

Please cite this article as: K. Verleysen, A. Parente and F. Contino, How does a resilient, flexible ammonia process look? Robust design optimization of a Haber-Bosch process with optimal dynamic control powered by wind, Proceedings of the Combustion Institute, https://doi.org/10.1016/j.proci.2022.06.027

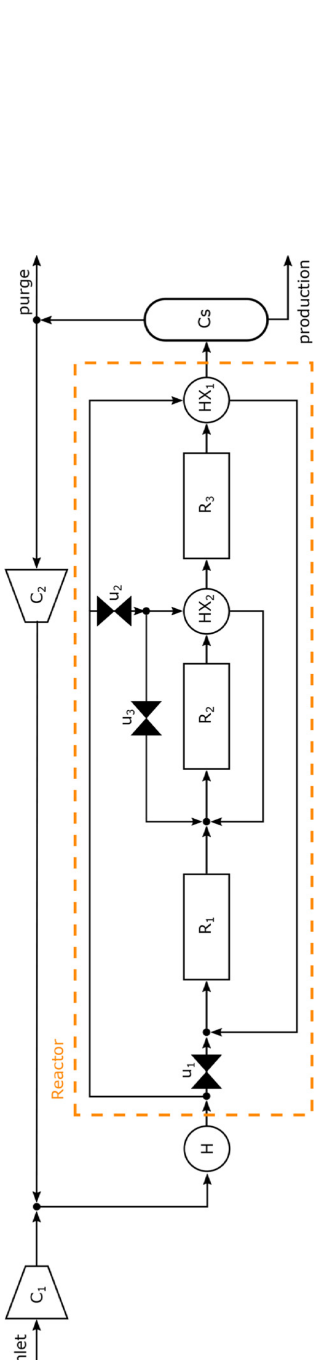

Fig. 1. The Haber-Bosch process consists of a loop compressor, the proposed reactor configuration, a separation system and a recycle compressor. These components are integrated in the Python library.

separation system by condensation (Cs), a purge stream and a recycle compressor (C_2). The recycle compressor compensates for the pressure drop in the condenser. The purge stream avoids the accumulation of inert gasses and a large recycle stream in the chemical process, which creates a large mass flow through the reactor and lowers the ammonia production at higher loads. In addition, this purge stream ensures the convergence of the recycle loop in the model, as is mentioned in Frattini et al. [38]. The integrated equations in the Python library for each component are extensively discussed in the thesis of Maria Brigitte Gullberg et al. [16]. The reactor model is represented by a plug flow reactor where the Temkin-Pyzhev rate reaction for an iron catalyst was combined with the molar and energy balance (partial differential) equations to simulate the behavior of the reactor over time. The adopted counter-current heat exchanger model uses the Number of Transfer Units (NTU) method to determine the temperature at the hot and cold outlets. We integrated an isentropic compressor model to calculate the needed work for a design outlet pressure. We combined the cooler and condenser model of Gullberg et al. and set the cooling temperature to 12.5 °C. The condenser model uses Raoult's law to calculate the molar fraction of the liquefied NH_3 based on the operational pressure and Henry's law to calculate the molar fractions of the condensed H_2 and N_2 [16]. For the dynamic simulation, we take the following assumptions:

- The loop pressure stays constant (we assume that the compressors have an ideal controller where the compressor power changes to compensate for any flow rate change).
- The preheater and cooling system has a constant output temperature (to avoid possible oscillation during the design optimization).
- The condenser model is always in steady-state.
- No pressure losses occur in the reactors, mixers, heat exchangers and heater.

We propose a reactor configuration which we then use to optimize the Haber-Bosch process in terms of production, flexibility, and resilience. This configuration cools the first and second reactor (R_1 and R_2) directly in combination with a heat exchanger (HX_1 and HX_2), while the third reactor (R_3) has an indirect cooling of the second heat exchanger (HX_2). The advantage of this configuration is that two valves (u_1 and u_3) control the temperature inlet for the first two reactors while valve u_2 controls the mass flow towards reactor R_2. The control of u_1 and u_3 allows us to go to lower loads as was described by Maria Brigitte Gullberg et al. [16] and Ostuni [39]. Reaching these lower loads (gaining higher flexibility) allows the HBS process to capture more renewable energy [5]. The inlet temperature of the third reactor is cooled, so the exothermic reaction is favored toward creating ammonia with Le Chatelier's principle.

2.2.3. Power management strategy

The chosen power management strategy always assumes a time delay between the first two products (H_2 and N_2) and the final product (NH_3). Meanwhile, the wind power production at time t must equal to the sum of the power towards each component (P_{PEM}, P_{PSA} and P_{HBS}) at time t. For this reason, we implemented the following strategy: the ammonia production at time t depends on the production of hydrogen and nitrogen from time $t-1$. With this inlet flow and the designed loop pressure, the necessary compression power (P_{HBS}) is known and extracted from P_{wind}. As was mentioned in Section 2.1, the wind power always covers the compression power at each timestep. The residual power (P_{wind} - P_{HBS}) is divided over the PEM and PSA according to a certain fraction that is chosen in the design optimization loop. The H_2 and N_2 streams (after buffering) are then provided to the HBS process for time $t+1$.

3. Optimization methodology

We introduce the objectives first in the optimization methodology. Next, a summary of the decision variables and constraints is provided. Finally, the robust design optimization and dynamic optimization are discussed.

3.1. Objectives

This paper aims to attain a PtA design resilient to temperature changes in the ammonia reactor and attain a high flexibility while having the maximum NH_3 production during load changes. According to Ganin et al. [40], resilience is a system's ability to absorb, respond and recover from disasters and adapt to new conditions. We defined the resilience in our case as the sum of absolute temperature changes at the outlet of the third reactor according to the steady-state value over time and divide this value by the number of timesteps (Eq. (12)).

$$\text{Resilience} = \frac{\sum_{i=1}^{3} V_i}{180} \int_0^{t_{\text{end}}} |T_o(t) - T_o(0)|\mathrm{d}t \qquad (12)$$

Therefore, resilience is, in our case, the thermal response of the ammonia catalyst to the wind power's disruptive behavior (via the hydrogen production and buffering) and the new conditions to the change in chemical equilibrium over time. This value has to be therefore minimized to create a resilient PtA process. To avoid an oversized volume reactor, we multiplied this value with the sum of reactor volumes to this equation. To measure the flexibility of the PtA plant, we define this objective as the ratio of the minimum NH_3 production over its maximum during each 3 h simulation (Eq. (13)).

$$\text{Flexibility} = \frac{\min(\dot{m}_{NH_3}(\forall t))}{\max(\dot{m}_{NH_3}(\forall t))} \qquad (13)$$

According to this definition, this value must be minimized to attain a flexible PtA process. As a third objective, we want to maximize the total accumulated NH_3 production over time. Therefore, we calculate the cumulative ammonia production over time, which must be maximized.

3.2. Design variables and constraints

We identified twelve design variables that directly affect the three chosen objectives. First, the volume of each reactor (V_i) needs to be sized, where a larger volume provides better NH_3 conversion but results in a more significant resilience. Then, the split fractions (u_i) of the NH_3 reactor and the purge fraction (u_{purge}) need to be designed such that the initial mass flows over the three reactors and the loop mass flow are optimized. When the loop mass flow is significant because of a small purge fraction (in combination with an improper reactor split fraction), the NH_3 production is reduced. Next, the loop pressure (p) and inlet reactor temperature (T_{Heater}) are defined such that the NH_3 production is favored, while the stability is guaranteed. Furthermore, the mass flow from the H_2 buffer tank ($\dot{m}_{H_2,cte}$), the power fraction to the PEM ($\%_{PEM}$), and the bypass flow fraction ($\%_{bypass}$) need to be designed because they directly affect the flexibility and NH_3 production. Finally, we implemented four constraints into the model, where for each reactor, the outlet temperature needs to have a minimum value and the total electric compression power can not be larger than 1 MW. These constraints avoid large mass flows (to a small purge fraction) or ineffective reactor configurations (reactor volumes and split fractions). We summarized these design variables and constraints in Table 1.

3.3. Robust design optimization

To the non-linearity of the PtA system, we implemented the Nondominated Sorting Genetic Algorithm (NSGA-II) to find the set of optimized design variables for optimizing the NH_3 production, resilience and flexibility. The NSGA-II is a multi-objective evolutionary algorithm that finds the optimized designs by evaluating the performance of a population and finds the most dominant design. A Pareto front can be formed between these objectives where a set of designs dominate every other set in at least one objective. The procedure to combine the PCE and NSGA-II is called a robust design optimization, where the goal of this procedure is to optimize the objectives (their mean values) while

Table 1
Design variables and constraints.

Design variable	Unit	Min	Max
V_1	[m^3]	0.1	3
V_2	[m^3]	0.1	3
V_3	[m^3]	0.1	3
u_1	[-]	0.1	0.25
u_2	[-]	0.1	0.7
u_3	[-]	0.1	0.95
u_{purge}	[-]	10^{-4}	0.1
p	[bar]	100	150
T_{Heater}	[°C]	70	90
$\dot{m}_{H_2,cte}$	[kg/s]	$2 \cdot 10^{-5}$	0.06
$\%_{PEM}$	[-]	0.9	1.0
$\%_{bypass}$	[-]	0	1
Constraint	Unit	Bound	
$T_{R_1,out}$	[°C]	min 400	
$T_{R_2,out}$	[°C]	min 350	
$T_{R_3,out}$	[°C]	min 400	
$\dot{W}_{net}$	[kW]	max 1000	

reducing the sensitivity of the objectives to the uncertainties (reducing the standard deviations) [41]. During the robust design optimization, we used 20 populations and a computational budget of 30 generations for the NSGA-II algorithm, a polynomial order p of 1 for the PCE and 100 uncertainties for the truncated KLE (N). We define this stage as the outer-loop optimization, where the NSGA-II searches the design space for the most optimal dynamic HBS process in the defined objectives.

3.4. Dynamic optimization

Within the dynamic PtA simulation, we implemented the nonlinear control and optimization mode of GEKKO [37]. Within this dynamic optimization, two control variables, i.e., valves u_1 and u_3, need to be manipulated such that, respectively, the inlet temperatures of the first and second reactor are constant at all times. This optimized control enables us to go to lower loads. The dynamic optimization in GEKKO calculates the L1-norm between the measured and objective value where the dynamic optimizer simultaneously optimizes multiple objectives in one optimization problem [42]. For this inner-loop optimization, the GEKKO optimizer adapts for each design at each timestep the two control variables to obtain a constant inlet reactor temperatures (reactor R_1 and R_2). The boundaries of these control variables (u_1 and u_3) are the same as the ones for the design variables (Table 1).

4. Results and discussion

This section shows the results of the robust design optimization of a PtA plant under stochastic wind power. We then discuss the key design variables that enable these designs.

The robust design optimization of the dynamic Power-to-Ammonia plant provides us with six Pareto fronts. These Pareto fronts are situated between four dominant designs, i.e. a most flexible design (lowest mean), a most productive design (highest mean), a most resilient (lowest mean) design and a robust flexible, resilient and productive (lowest standard deviation) design (Table 2). We observe a trade-off between the most productive and most flexible design where a 9.66% higher mean flexibility results in a 76.2% decrease in mean NH_3 production (Fig. 2). Also, the standard deviation of the flexibility decreases by 54.9% while the standard deviation of the NH_3 production decreases by 59.1%. We observe another significant trade-off between the most productive and robust design. Between these designs, there is a 54.1% decrease in NH_3 production and 14.2% less flexibility, while the standard deviations are 95.5% and 98.2% times lower for the respective objectives. Also, between the most flexible and robust cases, there is a 20.9% increase in flexibility with a 48.2% decrease in NH_3 production, while the standard deviations of these objectives increase 34.4 and 22.7 times, respectively.

For the resilience objective, we observe two trade-offs between three designs (Fig. 3). First, there is a significant trade-off between the most flexible and most resilient design, where there is a 17.2% less flexibility for a 5156 times higher resilience, 6704 times higher standard deviation for the flexibility and 375 times higher standard deviation for the resilience. A second more minor trade-

Table 2
The robust design optimization of the dynamic Power-to-Ammonia plant results in the best mean (μ) and lowest standard deviation (σ) for each objective. The most robust design has the lowest standard deviation in flexibility, resilience and NH_3 production.

		Most flexibility	Most resilience	Most productive	Robust flexibility, resilience and production
$\mu_{flexibility}$	[-]	0.787	0.951	0.871	0.994
$\sigma_{flexibility}$	[-]	0.036	$9.39 \cdot 10^{-3}$	0.023	$1.04 \cdot 10^{-3}$
$\mu_{resilience}$	[-]	4.908	0.093	2.245	2.336
$\sigma_{resilience}$	[-]	0.277	$4.07 \cdot 10^{-3}$	0.160	$1.00 \cdot 10^{-3}$
μ_{NH_3}	[MWh]	9.31	9.37	39.15	17.96
σ_{NH_3}	[MWh]	0.137	$28.9 \cdot 10^{-3}$	0.335	$6.04 \cdot 10^{-3}$

Please cite this article as: K. Verleysen, A. Parente and F. Contino, How does a resilient, flexible ammonia process look? Robust design optimization of a Haber-Bosch process with optimal dynamic control powered by wind, Proceedings of the Combustion Institute, https://doi.org/10.1016/j.proci.2022.06.027

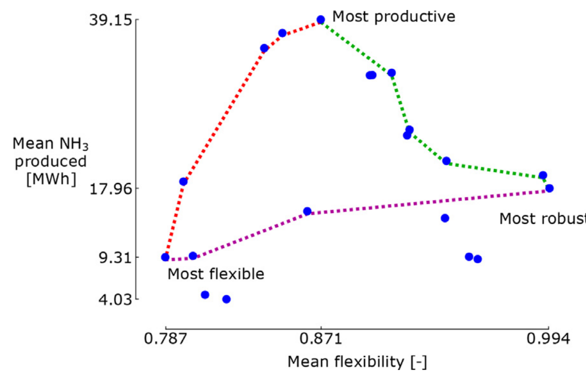

Fig. 2. The RDO provides three Pareto fronts between a productive, a flexible and a robust design.

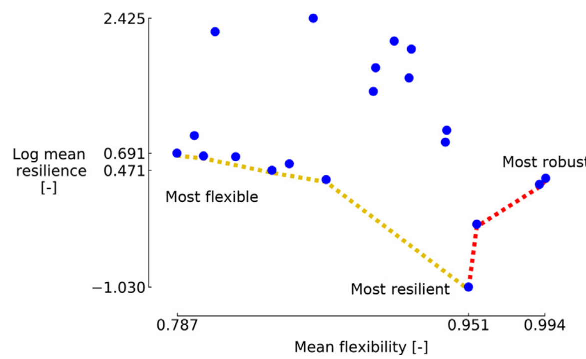

Fig. 3. The RDO provides two Pareto fronts between the most resilient, the most flexible and the most robust design.

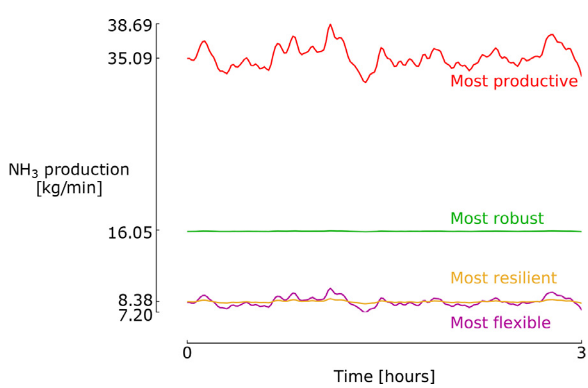

Fig. 4. The most productive, the most robust, the most resilient, and the most flexible designs provide different NH_3 flow rates for the same wind speed scenario.

off is between the optimal resilient design and the robust flexibility. Here, a 4.38% lower flexibility increases the resilience by 4.05 times, but decreases the standard deviation of the flexibility and resilience by 9.06 and 4.05 times, respectively.

These trade-offs originate from different design variables. The mean flexibility is proportional to the constant buffer feed ($\dot{m}_{H_2,cte}$) and reverse proportional to the bypass fraction ($\%_{\text{bypass}}$). This relationship shows that a flexible design requires a higher bypass fraction and a lower feed from the buffer tank. These two design variables have the reverse effect on the standard deviation of the flexibility, where a larger buffer feed and a smaller bypass fraction decrease the standard deviation. The mean and standard deviation of the resilience are proportionally linked to the sum of the volumes (V_i), the purge fraction (u_{purge}) and the temperature inlet of the reactor configuration (T_{Heater}). The definition of resilience links the reactor volumes to these values, while the purge fraction and the inlet temperature improve the resilience by changing the equilibrium condition, so the ammonia production is reduced but stable when there are power variations. The mean of the NH_3 production is directly linked to the bypass fraction and buffer feed, where increasing the feed and increasing the bypass fraction results in more significant total ammonia production. The standard deviation of the NH_3 production is proportionally linked to the bypass fraction because supplying the HBS process directly to the produced hydrogen links the NH_3 production direct to the stochastic wind power. The residual design variables (loop pressure, PEM fraction and split fractions) do not affect the Haber-Bosch performance in terms of robustness, resilience, production or flexibility.

With a single wind power scenario, we observe that the operation of the flexible and productive designs are similar (Fig. 4). In these designs, the variable wind power directly influences the ammonia production, but the NH_3 flow rate of the productive design is 4.18 times higher than the flexible design. The most robust and resilient designs resemble in operation, but the ammonia flow rate of the most robust design is 1.92 times higher than the flow rate of the resilient design. Between the resilient and most flexible design, we observe that mass flow rate is, on average, the same but presents a different operation.

5. Conclusion

Ammonia gains an essential role in the future energy transition. However, the NH_3 production via renewables is affected by the erratic nature of these resources. Combining stochastic renewable processes, like wind and solar, with a robust design optimization provides us with insight into how significant the effect of these energy sources have on a dynamic (chemical) process and reduces its sensitivity to uncertainty. This methodology can potentially optimize the design of electric power plants against erratic renewable power and variable demand, which will be the key to unlocking the potential of electrofuels. In this work, we used the Karhunen-Loève Expansion of the Ornstein-Uhlenbeck process to simulate wind power over three hours and used Polynomial Chaos Expansion to quantify the mean and standard deviation of the flexibility, resilience and NH_3 production of a dynamic Power-to-Ammonia plant. We coupled this method to the NSGA-II to optimize these objectives' mean and standard deviation. This procedure can be utilized to optimize the operation of any dynamic plant in the presence of renewable energy sources. We observed four extreme designs from the robust design optimization: an optimized mean flexible plant, an optimized mean productive plant, an optimized mean resilient plant, and a robust plant. Between each extreme design, there is a Pareto front of optimized designs, where several design variables, like the bypass fraction and buffer feed, are key elements for achieving these designs. In the future, we will perform this RDO of the PtA plant with more extended periods (days, weeks and months) and investigate its effect on the intermediate H_2 buffer size and the plant's cost.

Declaration of Competing Interest

The authors declare that they have no known competing financial interests or personal relationships that could have appeared to influence the work reported in this paper.

References

[1] IEA, Renewables 2020 – Analysis, Technical Report, IEA, 2020.
[2] D.O. Akinyele, R.K. Rayudu, Review of energy storage technologies for sustainable power networks, Sustainable Energy Technol. Assess. 8 (2014) 74–91.
[3] V. Dias, M. Pochet, F. Contino, H. Jeanmart, Energy and economic costs of chemical storage, Front. Mech. Eng. 6 (2020) 21.
[4] J. Ikäheimo, J. Kiviluoma, R. Weiss, H. Holttinen, Power-to-ammonia in future North European 100% renewable power and heat system, Int. J. Hydrogen Energy 43 (36) (2018) 17295–17308.
[5] J. Armijo, C. Philibert, Flexible production of green hydrogen and ammonia from variable solar and wind energy: case study of Chile and Argentina, Int. J. Hydrogen Energy 45 (3) (2020) 1541–1558.
[6] A. Valera-Medina, R. Banares-Alcantara, Techno-Economic Challenges of Green Ammonia as an Energy Vector, Academic Press, 2021.
[7] K. Verleysen, D. Coppitters, A. Parente, W. De Paepe, F. Contino, A. Parente, F. Contino, How can power-to-ammonia be robust? Optimization of an ammonia synthesis plant powered by a wind turbine considering operational uncertainties, Fuel 266 (2020) 117049.
[8] K. Verleysen, A. Parente, F. Contino, How sensitive is a dynamic ammonia synthesis process? Global sensitivity analysis of a dynamic Haber-Bosch process (for flexible seasonal energy storage), Energy 232 (2021) 121016.
[9] Institute for Sustainable Process Technology, ISPT, Power to Ammonia, Technical Report, ISPT, 2017.
[10] R. Bañares-Alcántara, G. Dericks III, M. Fiaschetti, P. Grünewald, J. Masa Lopez, E. Tsang, A. Yang, L. Ye, S. Zhao, Analysis of Islanded Ammonia-Based Energy Storage Systems, Technical Report, University of Oxford, Oxford, 2015.
[11] A. Allman, P. Daoutidis, Optimal scheduling for wind-powered ammonia generation: effects of key design parameters, Chem. Eng. Res. Des. 131 (2018) 5–15.
[12] R. Nayak-Luke, R. Bañares-Alcántara, I. Wilkinson, æGreeng ammonia: impact of renewable energy intermittency on plant sizing and levelized cost

of ammonia, Ind. Eng. Chem. Res. 57 (43) (2018) 14607–14616.
[13] I.I. Cheema, U. Krewer, Operating envelope of Haber–Bosch process design for power-to-ammonia, RSC Adv. 8 (61) (2018) 34926–34936.
[14] G. Wang, A. Mitsos, W. Marquardt, Renewable production of ammonia and nitric acid (2020), doi:10.1002/aic.16947.
[15] A. Jinasena, B. Lie, B. Glemmestad, Dynamic model of an ammonia synthesis reactor based on open information, in: Proceedings of The 9th EUROSIM Congress on Modelling and Simulation, EUROSIM 2016, The 57th SIMS Conference on Simulation and Modelling SIMS 2016, vol. 142, 2018, pp. 998–1004.
[16] R. Maria Brigitte Gullberg, V. Alstad, Y. International ASA, Controllability Analysis of Ammonia Synthesis Loops, Technical Report, 2018.
[17] A. Araújo, S. Skogestad, Control structure design for the ammonia synthesis process, Comput. Chem. Eng. 32 (12) (2008) 2920–2932.
[18] M.J. Palys, H. Wang, Q. Zhang, P. Daoutidis, Renewable ammonia for sustainable energy and agriculture: vision and systems engineering opportunities, 2021,
[19] H. Verdejo, A. Awerkin, E. Saavedra, W. Kliemann, L. Vargas, Stochastic modeling to represent wind power generation and demand in electric power system based on real data, Appl. Energy 173 (2016) 283–295.
[20] Y.H. Song, X.S. Chen, J. Lin, F. Liu, Y.W. Qiu, Stochastic processes in renewable power systems: from frequency domain to time domain, Sci. China Technol. Sci. 62 (12) (2019) 2093–2103.
[21] M. Olsson, M. Perninge, L. Söder, Modeling real-time balancing power demands in wind power systems using stochastic differential equations, Electr. Power Syst. Res. 80 (8) (2010) 966–974.
[22] Ø. BK, Stochastic Differential Equations: An Introduction With Applications, 5th edition, 1998.
[23] R.A. Maller, G. Müller, A. Szimayer, Handbook of financial time series, Handb. Financ. Time Ser. (2009) 421–437.
[24] M. Branickiy, A.J. Majdaz, Fundamental limitations of polynomial chaos for uncertainty quantification in systems with intermittent instabilities, Commun. Math. Sci. 11 (1) (2013) 55–103.
[25] E.B. Iversen, J.M. Morales, J.K. Møller, H. Madsen, Probabilistic forecasts of solar irradiance using stochastic differential equations, Environmetrics 25 (3) (2014) 152–164.
[26] Y. Qiu, J. Lin, X. Chen, F. Liu, Y. Song, Nonintrusive uncertainty quantification of dynamic power systems subject to stochastic excitations (2020).
[27] A. Loukatou, S. Howell, P. Johnson, P. Duck, Stochastic wind speed modelling for estimation of expected wind power output, Appl. Energy 228 (2018) 1328–1340.
[28] T. Schaffter, Numerical integration of SDEs: a short tutorial, 2010.
[29] C. Kahl, P. J, Numerical integration schemes for stochastic volatility models, Group February (2006).
[30] C. Kahl, P. Jäckel, Fast strong approximation Monte Carlo schemes for stochastic volatility models, Quant. Finance 6 (6) (2007) 513–536.
[31] L. Di Persio, G. Pellegrini, M. Bonollo, Polynomial chaos expansion approach to interest rate models, J. Probab. Stat. 2015 (2015).
[32] Y.C. Liang, H.P. Lee, S.P. Lim, W.Z. Lin, K.H. Lee, C.G. Wu, Proper orthogonal decomposition and its applications–Part I: theory, J. Sound Vibr. 252 (3) (2002) 527–544.
[33] S. Corlay, G. Pagès, Functional quantization-based stratified sampling methods (2014).
[34] A. Sánchez, M. Martín, Scale up and scale down issues of renewable ammonia plants: towards modular design, Sustain. Prod. Consum. 16 (2018) 176–192.
[35] A. Kashefi Kaviani, G.H. Riahy, S.M. Kouhsari, Optimal design of a reliable hydrogen-based stand-alone wind/PV generating system, considering component outages, Renew. Energy 34 (11) (2009) 2380–2390.
[36] E. Morgan, J. Manwell, J. McGowan, Wind-powered ammonia fuel production for remote islands: a case study, Renew. Energy 72 (2014) 51–61.
[37] L. Beal, D. Hill, R. Martin, J. Hedengren, Gekko optimization suite, Processes 6 (8) (2018) 106.
[38] D. Frattini, G. Cinti, G. Bidini, U. Desideri, R. Cioffi, E. Jannelli, A system approach in energy evaluation of different renewable energies sources integration in ammonia production plants, Renew. Energy 99 (2016) 472–482.
[39] Ostuni, Method for load regulation of an ammonia plant(2008).
[40] A.A. Ganin, E. Massaro, A. Gutfraind, N. Steen, J.M. Keisler, A. Kott, R. Mangoubi, I. Linkov, Operational resilience: concepts, design and analysis, Sci. Rep. 6 (2016) 1508.01230, doi:10.1038/SREP19540.
[41] D. Coppitters, W. De Paepe, F. Contino, Robust design optimization of a photovoltaic-battery-heat pump system with thermal storage under aleatory and epistemic uncertainty, Energy 229 (2021) 120692.
[42] J.D. Hedengren, R.A. Shishavan, K.M. Powell, T.F. Edgar, Nonlinear modeling, estimation and predictive control in APMonitor, Comput. Chem. Eng. 70 (2014) 133–148.